Nanoscale

Photo-Induced Electrodeposition of Metallic Nanostructures on Graphene

Journal:	*Nanoscale*
Manuscript ID	NR-ART-02-2020-000934.R1
Article Type:	Paper
Date Submitted by the Author:	27-Mar-2020
Complete List of Authors:	Xia, Kangwei; Katholieke Universiteit Leuven, Department of Chemistry Chiang, Weiyi; Katholieke Universiteit Leuven, Department of Chemistry; National Chiao Tung University, Department of Applied Chemistry Lockhart de la Rosa, César; Katholieke Universiteit Leuven, Department of Chemistry Fujita, Yasuhiko; KULeuven, Chemistry Toyouchi, Shuichi; KULeuven, Chemistry Yuan, Haifeng; Katholieke Universiteit Leuven, Department of Physics Su, Jia; South University of Science and Technology of China Masuhara, Hiroshi; National Chiao Tung University, Laser Bio/Nano Science De Gendt, Stefan; imec, De Feyter, Steven; Katholieke Universiteit Leuven, Department of Chemistry Hofkens, Johan; KULeuven, Division of Molecular Imaging and Photonics, Department of Chemistry Uji-i, Hiroshi; Hokkaido University, Research Institute for Electronics Scince (RIES); KU Leuven, Chemistry

ARTICLE

Photo-Induced Electrodeposition of Metallic Nanostructures on Graphene

Received 00th January 20xx,
Accepted 00th January 20xx

DOI: 10.1039/x0xx00000x

Kangwei Xia [a+*], Wei-Yi Chiang[a,b+], Cesar Javier Lockhart de la Rosa[a,c+], Yasuhiko Fujita[a], Shuichi Toyouchi[a], Haifeng Yuan[a], Jia Su[a,d], Hiroshi Masuhara[b,e], Stefan De Gendt[c,f], Steven De Feyter[a], Johan Hofkens[a], Hiroshi Uji-i[a,g*]

Graphene, a single atomic layer of sp^2 hybridized carbon, is a promising material for future devices due to excellent optical and electrical properties. Nevertheless, for practical applications, it is essential to deposit patterned metal on graphene in the micro and nano-meter scale in order to inject electrodes or modify the 2D film electrical properties. However, conventional methods for depositing patterned metal such as lift-off or etching leave behind contamination. This contamination has been demonstrated to deteriorate the interesting properties of graphene such as its carrier mobility. Therefore, to fully exploit the unique properties of graphene, the controlled and nano-patterned deposition of metals on graphene films without the use of a sacrificial resist is of significant importance for graphene film functionalization and contact deposition. In this work, we demonstrate a practical and low-cost optical technique of direct deposition of metal nano-patterned structures without the need for a sacrificial lift-off resist. The technique relies on the laser induced reduction of metal ions on a graphene film. We demonstrate that this deposition is optically driven, and the resolution is limited only by the diffraction limit of the light source being used. Patterned metal features as small as 270 nm in diameter are deposited using light with a wavelength of 532 nm and a numerical aperture of 1.25. Deposition of different metals such as Au, Ag, Pd, Pb and Pt is shown. Additionally, change of Fermi level of the graphene film through nano-patterned metal is demonstrated through the electrical characterization of four probe field effect transistors.

1. Introduction

Graphene, a 2D material based on a single atomic layer of sp^2 hybridized carbon,[1] has been of great interest for diverse applications ranging from transparent electrodes, (opto)electronic devices, and high radio frequency electronics to energy storage and biological sensors.[2-6] This interest was mainly driven by its ultrathin-body, excellent mechanical and thermal properties and unique electronic properties such as very high ambipolar mobility as well as its optical properties.[7,8] Most of these properties often degrade as the graphene film is exposed to chemical contaminations during fabrication processes.[9] Several groups have already addressed the reduction of contamination during high-quality CVD growth of graphene and the transfer of graphene films to dielectric substrates.[10-12] Nevertheless, the process of controlled and patterned deposition of metals on the graphene film and contaminations possibly induced during the process have received less attention up to now. This process is of foremost importance for an extensive range of applications such as graphene plasmonics, photodetectors and field effect transistors, not only for contacting the graphene but also for functionalizing its surface and changing its (opto)electronic properties for purposes such as carrier doping at nanoscale.[13] Currently, the fabrication process of electrodes on graphene is done by depositing metals through a lift-off process with the aid of a sacrificial resist. The resist could additionally introduce chemical contamination on the graphene surface.[14] Thus, it is of great interest to be able to selectively deposit the metal without use of a sacrificial resist. Furthermore, patterned metal deposition is a crucial process also for making an electrical contact on the graphene film. For this, it has been reported that the presence of sp^3 bonds at the edges of graphene could be of benefit to reduce the contact resistance.[15]

[a.] *Laboratory for Photochemistry and Spectroscopy, Division for Molecular Imaging and Photonics, Department of Chemistry, KU Leuven, Celestijnenlaan 200F, B-3001 Leuven, Belgium*
[b.] *Department of Applied Chemistry, National Chiao Tung University, Hsinchu 30010, Taiwan*
[c.] *Imec, Kapeldreef 75, B-3001 Leuven, Belgium.*
[d.] *Department of Biology, South University of Science and Technology of China, Shenzhen 518055, China*
[e.] *Center for Emergent Functional Matter Science, National Chiao Tung University, Hsinchu 30010, Taiwan*
[f.] *Molecular Design and Synthesis, Department of Chemistry, KU Leuven, Celestijnenlaan 200F, B-3001 Leuven, Belgium*
[g.] *RIES, Hokkaido University, Sapporo, 001-0020, Japan*

† Equal contributions
*Corresponding authors: Kangwei Xia kangweixia@gmail.com, Hiroshi Uji-i hiroshi.ujii@kuleuven.be
Electronic Supplementary Information (ESI) available: [details of any supplementary information available should be included here]. See DOI: 10.1039/x0xx00000x

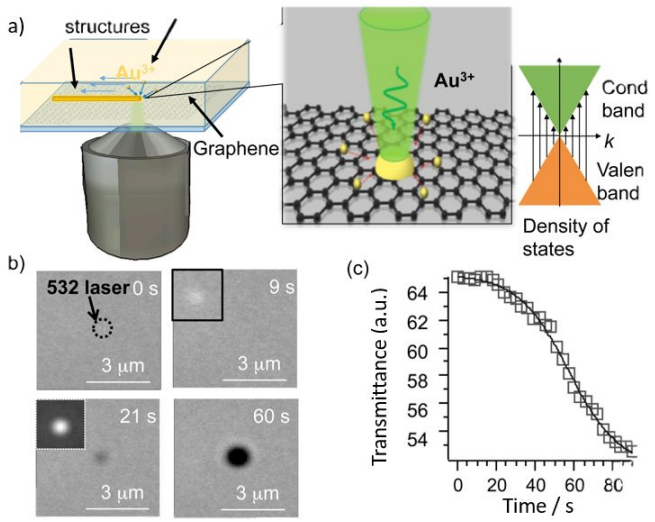

Figure 1 (a)Experimental scheme and system. Different metals can be nano-graphed on graphene due to photo-induced electron-hole production. (b) Sequential transmittance and Rayleigh scattering images during gold deposition. The transmittance images are recorded with the laser off. The Rayleigh scattering images, shown as insets of the transmittance images, are recorded with the laser on. (c) Plot of the transmittance at the focus against laser irradiation time.

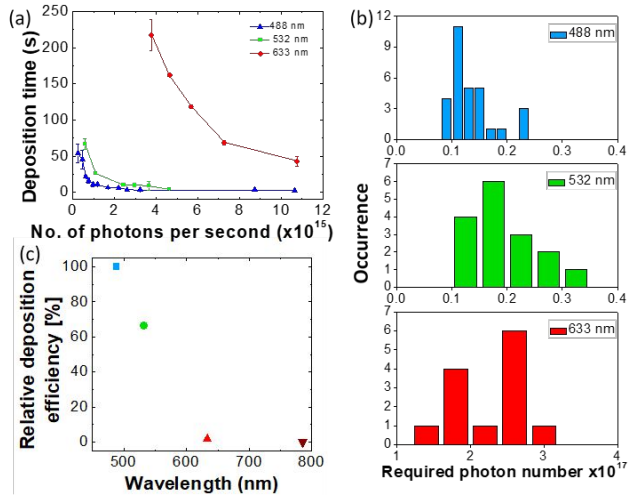

Figure 2 (a) Relation between laser power and onset of deposition (see text) for three different wavelengths. The laser power was converted to photon number per second. (b) Required photon number to induce the deposition was calculated from (a) as (onset of deposition) × (number of photons per second). (c) Relative deposition efficiency (see text) at each wavelength, obtained by normalizing the efficiency of 488 nm laser deposition to 100 %.

Very recently, ice lithography, which uses water ice as resists, has been demonstrated for fabrication of metal nanostructures on graphene.[16] It requires high vacuum and a sequential electron beam lithography process. A more practical and low-cost approach is desired to directly deposit different types of metals on graphene films without the use of sacrificial resist. Here, we demonstrate a direct and simple method to *in-situ* site-specifically deposit metal on graphene with sub-micrometre precision by light. Metals including Au, Ag, Pt, Pd and Pb have been successfully deposited on graphene surface from a metal ion aqueous solution by locally ionizing graphene upon focusing laser light on the surface. This has been achieved likely through temporal increase of the local electron concentration in the conduction band of graphene upon light irradiation with appropriate wavelengths. We propose that electrons pumped into the conduction band of graphene likely induce the reduction of metal ions delivered in solution leading to metal deposition at the laser focus spot. We first study the mechanism of the photon-induced metal deposition process on graphene, showing that this process is universal to various metal nanoparticles (NPs). This all-optical approach offers a new platform to locally engineer graphene with nanometre precision and cost-effectiveness. Finally, we demonstrate local doping of graphene and the possibility to electrically contact the graphene film by reading out electrically modified graphene based field effect transistors (FETs).

2. Results and discussions

We hypothesize that the mechanism of the patterned deposition of metal on a single layer of graphene is initiated by the photo-induced electron-hole production of graphene as illustrated in Fig. 1a. To assess this hypothesis, a graphene-on-glass substrate covered with an aqueous solution of $HAuCl_4$ was subjected to either wide-field optical transmission and luminescence/scattering microscopy or confocal Raman spectroscopy (experimental details can be found in the Supplementary Materials Fig. S1 and Note 1, 2). Briefly, a CW laser beam was focused at graphene/liquid interface to induce electron-hole reduction on graphene. In this experiment, the laser on/off status was controlled by a mechanical shutter. Transmission (laser off) and luminescence/scattering (laser on) images at the laser focus were captured by means of wide-field optical transmission/luminescence microscopy, while the Raman spectra of graphene were recorded with confocal Raman spectroscopy (Note that the obtained Raman spectra may include also luminescence/scattering signals from the deposited metals).

Table 1, Photon energy, photon numbers to reach the visible spots, and deposition efficiency as a function of excitation wavelength. The reduction energy of gold ions is 1.69 eV.

Laser wavelength nm	Photon energy eV	Photon numbers	Deposition efficiency / %
488	2.54	1.33×10^{16}	100%
532	2.33	1.97×10^{16}	68%
633	1.96	2.26×10^{17}	6%
785	1.58	--	--

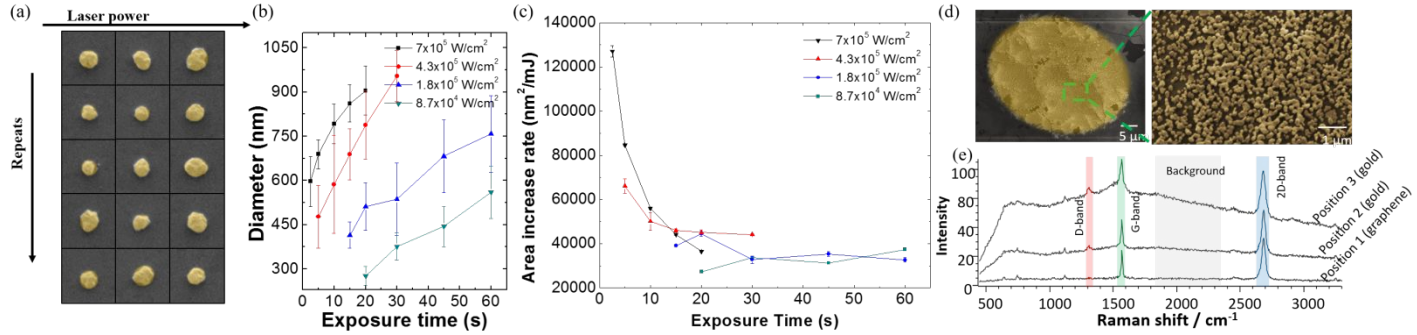

Figure 3 SEM image of individual deposited gold nanoparticles on graphene with different laser irradiation powers at 532 nm. The scale bar is 1 μm. (b) Diameter of deposited gold nanoparticles for different exposure power and time. (c) The growth rate (see text) was plotted against exposure time for different laser power. (d) Left graph, SEM image of gold deposition under wide-field light irradiation. Right graph, its zoom-in image. (e) Time dependent Raman spectra. Position 1 corresponds to the initial state of graphene without gold deposition. Position 2 and 3 is a gold deposition area after a few seconds and one minute of irradiation, respectively.

Before light irradiation (at 0 s), the graphene sample does not show any features in the optical transmission image (Fig.1b), suggesting a smooth surface of graphene. After 20 s laser irradiation, a disk-shaped dark region gradually appears at the focus in the transmission image (left bottom in Fig.1b). Upon continuous laser irradiation, the transmittance around the laser focus decreases as function of time (Fig. 1c) and the dark disk increases in size as can be seen in the time-lapse imaging in Fig. 1b. By measuring luminescence image, we notice strong light scattering (mainly Rayleigh scattering) from the focus region (see the insets in Fig. 1b). Already at 9 s, slight scattering was observed in the luminescence image (the inset of the upper-right image in Fig. 1b), while nothing was visible in the transmission image. This suggests that something smaller than the diffraction limit with large light cross section is growing at the light focus position. We assume that gold metal was deposited on the graphene surface upon illumination (*vide infra*).

Rayleigh scattering intensity relates to the amount of the metal NPs deposited on surface.[17] In our experiment, scattering intensity increases as function of time, indicating increase in the number of metal NPs at the focus position. Furthermore, a sigmoid function fits the transmittance profile curve at the focal spot over the period of light excitation (Fig. 1c). This implies solid-state kinetics of nucleation at the laser focus on graphene.[18] Thus, we deduce that the observed object is formed by local reduction of gold ions through the local electronic excitation of graphene. Control experiments with a salt free solution and/or graphene do not give rise to these changes both in transmittance and scattering, suggesting that metal NPs deposition through the photo-induced local reduction of metal ions in the presence of graphene is responsible for this change. Given the crossing of the valence and conduction band of graphene at the Dirac points, electrons in the valence band can be easily excited to the conduction band upon light irradiation. This process is commonly known as photo-induced electron-hole formation.[19] The photo-electrons can reduce the metal ions at the solution/graphene interface, resulting in local metal deposition on graphene. Hereafter we abbreviate this photo-induced-metal-deposition as PIMD.

To comprehend the process of PIMD on graphene, the NPs deposition efficiency has been investigated as a function of excitation wavelength (energy) and number of photons to deposit visible spots at four different wavelengths, i.e. 488 nm (2.54 eV), 532 nm (2.33 eV), 633 nm (1.96 eV) or 785 nm (1.58 eV). The number of photons was controlled to be in the range of 10^{16}-10^{17} for all wavelengths. First, the dependences were examined for an Au^{3+} containing solution on graphene. The onset time of Au NPs deposition as function of photon number at each wavelength as determined by means of Raman spectroscopy is plotted in Fig. 2a. The Raman spectrum of pristine graphene shows only the characteristic G-band and 2D-band. After starting the laser irradiation, the D-band appears,

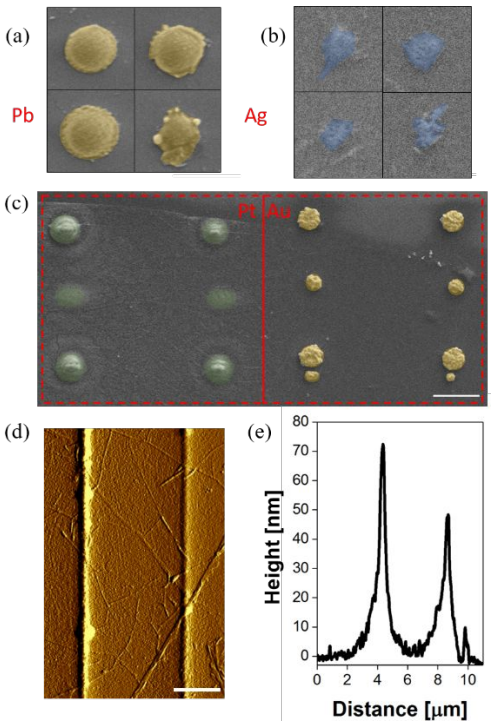

Figure 4 (a) SEM image of deposited Pb nanoparticles on graphene. (b) SEM image of deposited Ag nanoparticles. (c) SEM image of deposited Pt and Au nanoparticles, indicating the ability of dual metal nano-graphing. (d) AFM image of as-grown Pt nanolines. (e) Height profile of the Pt nano-line. All scale bars correspond to 1 μm.

indicating local changes in the hybridisation of the carbon atoms of graphene (from sp^2 to sp^3 (see Fig. 3e)). Additionally, the background signal increases in time, which is most likely due to scattering/luminescence of Au NPs. The time to detect the D-band and background signal is defined as onset time of deposition in this study. For all excitation wavelengths, we found shorter onset time at higher laser power. With respect to the photon energy dependence from Fig. 2a 488 nm laser irradiation requires the shortest time to gold nanoparticle deposition, while it takes slightly longer (a few seconds) at 532 nm excitation. In contrast, the onset time at 633 nm increased twofold. Notably, using a 785 nm laser, we hardly observed any gold deposition on graphene.

Based on the onset time at each wavelength in Fig. 2a, we calculated the required photon number to give detectable deposition for each experiment (Fig. 2b and Tab. 1). The required photon number was calculated by multiplying the onset time with the photon flux. The total number of photons required for the Au deposition shows wavelength dependence: 1.33×10^{16}, 1.97×10^{16} and 2.26×10^{17} for 488 nm, 532 nm and 633 nm, respectively. Additionally, we determined the relative deposition efficiency for each wavelength (Fig. 2c) that is defined as the ratio, expressed in %, of the required photon number at 488 nm divided by the required photon number for deposition at a given wavelength. Accordingly, the relative deposition efficiency at 532 nm is 68 % and at 633 nm only 6 % (details see the Supplementary Materials Note 3). Although the photon energy of 785 nm light (1.58 eV) is higher than the reduction energy of Au^{3+} to Au (1.50 eV),[20] no detectable PIMD was observed with 785 nm light, that is 0 % of the relative deposition efficiency. This indicates that the PIMD demonstrated here for Au proceeded via multiple reaction steps as proposed in other studies on photo-induced Au reduction.[21] 1. At the beginning, electron-hole pairs are generated on graphene by light irradiation. 2. The electrons, which have a higher energy than (carriers near) the Fermi level (so-called hot electrons), reduce Au^{3+} to Au^{2+} at graphene/solution interface (Eq.1). 3. Then reaction proceeds via disproportionation (Eq.2). 4. Au+ ion is further reduced by hot electrons with reduction energy of 1.69 eV.[20] Thus, 785 nm (1.58 eV) light cannot complete the final step.

$$HAu^{3+}Cl_4 + e^-(\text{graphene}) \rightarrow HAu^{2+}Cl_3 + Cl^- \quad (1)$$
$$2HAu^{2+}Cl_3 \rightarrow HAu^{3+}Cl_4 + HAu^{+}Cl_2 \quad (2)$$
$$HAu^{+}Cl_2 + e^-(\text{graphene}) \rightarrow Au^0 + HCl + Cl^- \quad (3)$$

Spatial resolution of the deposition is important for future applications. Thus, we have determined the resolution of our PIMD of gold NPs by focusing 532 nm laser beam with a 1.25 NA oil objective at the solution/graphene interface. Figure 3a shows SEM images of individual deposited gold NPs at different laser power and irradiation time. Size of gold NPs is reasonably reproducible and the smallest size here is about 270 nm, indicating that the minimum size is determined by the diffraction limit of the optical system. The size of the gold NPs against the exposure time is presented in Fig. 3b. (We also demonstrated the gold NP deposition with 0.6 N.A. air objective lens. Results are presented in the Supplementary Materials Note 3.) Longer exposure time or higher irradiation laser power result in an increase of the diameter of the deposited gold NPs.

In order to study the impact of exposure time and excitation power on the increase of the deposition area during the PIMD process, we define the area increase rate as area/[(exposure time)×(photon density)]. We plot it as a function of the exposure time for different laser power (Fig. 3c). At high laser power, the deposition process is fast at short exposure time, and the area increase rapidly slows down with exposure time, showing saturation behaviour within 20 s. At low laser power, longer exposure time is required to achieve deposition, and the area increase rate gradually decreases with exposure time. From Fig. 3c, two different tendencies can be identified according to the laser power used and the area increase rate. First, the area increase rates decrease with exposure time at any laser power. At the very beginning of the PIMD process the ionization of graphene by the light irradiation induces the growth of the Au particle. After Au particle is formed on the graphene, however, the particle itself hinders the growth by scattering and absorbing the laser light, and spacing between graphene surface and salt solution. Thus, the area increase rate slows down with increasing size of the Au particle. Second, in the low laser power range (8.7×10^4 W/cm^2 and 1.8×10^5 W/cm^2), the area increase rate is less dependent on the exposure power. On the other hand, when the irradiation laser power is high (4.3×10^5 W/cm^2 and 7×10^5 W/cm^2), the area increase rate is rapidly decreasing, and shows remarkable laser power dependence, indicating that the generated heat has a significant impact on the growth process. This behaviour can't be explained by the PIMD process alone. Some factors should be considered such as depletion of gold ions at surface layer and additional thermal convection. For example, the diffusion of gold ions from surrounding to deposited area might not be fast enough and high density of electrons on graphene surface may induce strong electron repulsion leading to electron scattering out from deposition area. It indicates that after the seed is formed, not only the PIMD, but some other mechanisms such as thermal convection and repulsion effects influence the efficiency of the gold growth.

Metal deposition at large area was achieved through wide-field irradiation (Fig. 3d). After 5 minutes of irradiation, gold nanoparticles started to emerge in the irradiated area and, finally, a homogeneous gold region with sharp edges was formed, of which a SEM image is shown in the left panel of Fig. 3d. The zoom-in SEM image of the gold deposition induced by the wide-field illumination is presented in the right panel of Fig. 3d, where individual 200 nm sized nanoparticles of gold can be found. This offers the interesting prospect of patterning gold on nanographene, for instance using photomasks.

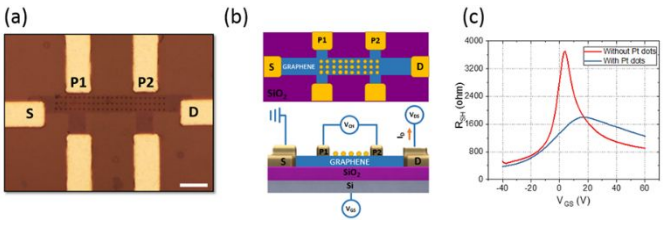

Figure 5 (a) Optical image of a four-probe device after functionalization with PIMD Pt dots. The scale bar is 10 μm. (b) Top and cross-sectional Schematic of the setup for four-probe measurements. (c) Transfer characteristics of the four-probe devices before and after functionalization.

Hyper-spectral Raman mapping images of graphene after gold deposition are shown in the Supplementary Materials Note 3. The scattering signal appears only on the gold deposited spots. The G- and 2D-bands increase in intensity, most likely because of Raman scattering enhancement due to the localized surface plasmon resonance of the deposited gold NPs. Additionally, we observed an increase in the intensity of the graphene D-band as function of irradiation time, indicating that defects in the graphene lattice were created during the PIMD. It indicates that for the deposition of Au on graphene, laser irradiation changes the hybridisation of the C-atoms in graphene from sp^2 to sp^3. [22,23]

In order to extend the PIMD technique to applications, a universal approach to different kinds of metals and deposited structures is indispensable. We further successfully induced Pb, Ag, Pt, and Pd deposition on graphene by irradiating the graphene surface with a 532 nm laser (the laser power was ~10^5 W/cm^2 range) while the graphene-on-glass substrate was submerged in the respective metal-salt containing solution with experimental details in the Supplementary Materials Note 4-7. The SEM images of deposited Pb, Ag, Pt nanoparticles are displayed in Fig. 4a-c. The reduction energy of Ag, Pb, and Pt is 1.2 eV, 0.126 eV and 0.987 eV, respectively. [20] Those metal elements were also determined by energy dispersive spectroscopy (EDS) measurements as shown in Supplemental Materials Note 4-7. We also demonstrated compositional control in combination with positional control. For instance, after the on-graphene growth of Au NPs, the sample was washed with pure water, and exposed to a solution of Pt salt, allowing the controlled deposition of Pt particles adjacent to Au particles using the PIMD approach (Fig. 4c). On the other hand, laser irradiation of Au/Pt mixture solution results in the deposition of only Au NP on graphene due to the difference in ionization tendency between Au and Pt as shown in the Supplementary Materials Note 8. This novel method of depositing different metal particles on graphene with nanometer precision offers a new platform to *in situ* nanograph metallic nanostructures. The deposition of the metal nanostructures is not limited to domelike structures. Nanolines were deposited as well as demonstrated for Pt (see Fig. 4d and 4e). The patterned lines prove nice controllability of linewidth and thickness; 400 nm linewidth with 70 nm thickness. Such performance is comparable to conventional photolithography (typically 365 nm) using photoresists.

3. Device application of metal nanostructures on graphene

After studying the mechanism of PIMD metal deposition we investigated the impact of PIMD deposited metal lines under field effect transistors (FET) contacts. As the PIMD deposited metal lines do not require resist or lift-off, the interface of the PIMD deposited metal itself with the graphene have very reduced amount of contamination. In addition, the increase in the D peak of the Raman spectra after PIMD functionalization indicates emergence of sp^3 hybridization. This gives edge-like contacts to graphene without complicated processing or patterning of the graphene before contact deposition as done and required in previous works.[24-26]

The results can be seen in Fig. S18 of the Supplementary Materials Note 9. The contact resistance (R_C) and the sheet resistance (R_{SH}) where extracted using the transfer length method (TLM). From the extracted values it was seen that R_C is marginally affected by the introduction of the PIMD lines (~50 ohm*µm change). The lack of a considerable reduction in R_C as it would have been expected from the introduction of edge contact can be explained by the non-ideal chosen alignment of the PIMD lines that could limit the injection of carriers from the lines far from the channel. Nevertheless, the fact that the value remains similar is a demonstration that the technique could be used as a replacement to conventional lift-off metal deposition process.

Table 2 Extracted parameters from 4P-FET before and after PIMD Pt dots functionalization.

	Before	*After PIMD Pt dots*
V_K *(V)*	4	15
N_{2D} *(cm^{-2})*	9.5×10^{11}	35.6×10^{11}
Mobility hole (cm^{2}V^{-1}s^{-1})	1487	1498
Mobility electrons (cm^{2}V^{-1}s^{-1})	561	183

Next, we explored the use of PIMD patterned metal structures on the graphene sheet to modify its (photo)electronic properties without resist cross-contamination at the graphene-metal interface. For this purpose, graphene back-gated four-probe field effect transistors (4P-FET) were fabricated using same technique previously described in literature.[22] The after-built devices were cleaned in acetone at 50°C for 4 hr, dipped in isopropyl alcohol followed by N_2 blow drying. The devices were functionalized by depositing Pt dots on the graphene channel through PIMD (Fig. 5a). Finally, the devices were electrically characterized by applying a potential (V_{DS}) between the source (S) and drain (D) electrodes and modulating the current circulating through the graphene sheet (I_D) by changing the back-gate potential (V_{GS}). In addition to I_D, the potential drop across the graphene channel ($V_{P2\text{-}P1}$) is measured through the potential electrodes (P1 and P2). A schematic of the setup is given in Fig. 5b. The sheet resistance (R_{SH}) of the devices is extracted without the effect of parasitic metal/graphene contact by using $R_{SH} = (W_{CH}/L_{CH})\ (V_{CH} / I_D)$, where W_{CH} is the channel width and LCH is the distance between P1 and P2 (25 µm).

The extracted R_{SH} for the functionalized and the non-functionalized devices is given in Fig. 5c. In an ideal graphene device RSH should tend to infinite at the neutrality point (R_{SH} peak). However, due to charge impurities that create electron-hole puddles, in a real graphene FET a finite resistance is always achieved.[27] Therefore, the decrease of the maximum RSH for the sample after functionalization with PIMD Pt dots can be explained by an increase of impurities/defect (such as sp^3 bond formations as previously observed from Raman) in the film after functionalization. The right shift observed at the neutrality point on the functionalized samples follows the expected increase in hole concentration (p-doping) from the Pt functionalization demonstrating the possibility to control the

Fermi level of the graphene sheet through nano-metal decoration. This was previously observed for Pt functionalized samples but with high coverage (particles bigger than 500nm) using a much more complicated deposition technique.[28,29] To better understand the effect of the PIMD deposited Pt dots, the carrier mobility was extracted as $\mu_{4P\text{-}FET} = (dG_{SH}/dV_{GS})\ (1/C_{OX})$ where $G_{SH} = 1/R_{SH}$ and C_{OX} is the oxide capacitance (3.80×10^{-8} F·cm^{-2}). Also, the carrier concentration at the K point (N_{2D}) of the devices was obtained as $N_{2D} = (V_K\ C_{OX})/q$ where VK is gate potential, and q is the electron charge (1.60×10^{-19} C). The extracted values can be seen in Table 2. Interestingly, the hole concentration increased from 9.5×10^{11} cm^{-2} to 35.6×10^{11} cm^{-2} as expected from p-type doping. More importantly, the extracted hole mobility remained almost constant (1487 cm^{2}V^{-1}s^{-1} vs 1498 cm^{2}V^{-1}s^{-1}). Thus, the PIMD method can be used to efficiently tailor the electronic properties of graphene devices such as its Fermi level. We also evaluated the impact of PIMD metal lines in the contact of field effect transistors and showed the details in the Supplementary Materials Note 9.

4. Conclusions

The deposition of several metal nanoparticles or line structures on single graphene layer was carried out by laser irradiation through a solution of metallic salts, where the reduction of metal ions is made possible by produced electron-hole on graphene. As we have demonstrated, Au, Ag, Pt, Pb or Pd nanoparticles are formed on graphene by means of a locally controlled deposition using a focused laser beam. Besides, deposition of multiple metals is realized in the same area. Additionally, PIMD deposited nanoparticles were used to successfully functionalize the graphene film showing successful doping of the film after the metal deposition.

The method here presented enables the deposition of patterned metal structures for contacting graphene or for manipulating the graphene Fermi level without the need for lift-off like processes, thereby reducing contamination risk and opening a new way for graphene-based materials processing. The concept of electron-hole production could also be useful for other functionalization protocols of graphene where ionization of the surface is required such as molecular grafting.

Conflicts of interest

There are no conflicts to declare

Acknowledgements

The authors acknowledge financial support from the Research Foundation - Flanders (FWO Grant numbers G.0D45.19N, G.0B55.14N, G.0819,16N, G.0B39.15, G.0B49.15, G098319N and ZW15_09-GOH6316, the KU Leuven Research Fund (C14/15/053), the Flemish government through long term structural funding Methusalem (CASAS2, Meth/15/04), the Hercules foundation (HER/11/14), the Nakatani Foundation, JST PRESTO program, the European Research Council under the European Union's Seventh Framework Programme (FP7/2007-2013)/ERC grant agreement no. 291593 to J.H.; 340324 to S.D.F.; and 280064 to H.U., JSPS Kakenhi (JP17H03003, JP17H05244, JP17H05458) and the JSPS Core-to-Core Program. Support in the form of Advanced Research Networks to H.U. is gratefully acknowledged. H. M. acknowledges support from The Featured Areas Research Center Program within the framework of the Higher Education SPROUT Project by the Ministry of Education (MOE) in Taiwan and the Ministry of Science and Technology (MOST) in Taiwan (MOST 107-2113-M-009-013).

References

1 K. S. Novoselov, A. K. Geim, S. V. Morozov, D. Jiang, Y. Zhang, S. V. Dubonos, I. V. Grigorieva, A. Firsov; *Science*, 2004, **306**, 666.
2 M. Chae, T. Lee, K. Son, Y. Kim, K. Hwang, T. Kim; *Nanoscale Horiz.,* 2019, **3**, 610-618.
3 S. Islam, J. Mishra, A. Kumar, D. Chatterjee, N. Ravishankar, A. Ghosh; *Nanoscale*, 2019, **11**, 1579-1586.
4 A. Ferrari, *et.al*., *Nanoscale*, 2015, 4598-4810.
5 J. Xie, C. C. Guo, M. Li, *Energy Environ. Sci*., 2014, **7**, 2559.
6 R. Zhou, C. Wang, W. Xu, L. Xie; *Nanoscale,* 2019, **11**, 3445-3457.
7 A. H. Castro Neto, F. Guinea, N. M. R. Peres, K. S. Novoselov, and A. K. Geim; *Rev. of Mod. Phys.*, 2009, **81**, 109–162.
8 F. Bonaccorso, Z. Sun, T. Hasan & A. C. Ferrari; *Nat. Photonics,* 2010, **4**, 611–622.
9 A. Pirkle, J. Chan, A. Venugopal, D. Hinojos, C. W. Magnuson, S. McDonnell, L. Colombo, E. M. Vogel, R. S. Ruoff, and R. M. Wallace; *Appl. Phys. Lett.,* 2011, **99**, 122108.
10 L. Banszerus, M. l. Schmitz, S. Engels, M. Goldsche, K. Watanabe, T. Taniguchi, B. Beschoten, C. Stampfer*; Nano Lett.,* 2016, **16**, 1387-1391.
11 K. Verguts, B. Vermeulen, N. Vrancken, K. Schouteden, C. Van Haesendonck, C. Huyghebaert, M. Heyns, S. De Gendt, S. Brems; *J. Phys. Chem. C,* **120** , 297-304.
12 C. Lockhart de la Rosa, J. Sun, N. Lindvall, M. T Cole, Y. Nam, M. Löffler, E. Olsson, K.Teo, A. Yurgens; *Appl. Phys. Lett.,* 2013, **102** , 022101.
13 B. Jiang, Q. Wu, L. Zhang, Y. Zhanga; *Nanoscale*, 2017,**9**, 1607-1615.
14 B. Kantar, M. Öztürk, H. Çetin, *Bull. Mater. Sci.,* 2017, **40**, 239-245.
15 14. H. Park, W. Jung, D. Kang, J. Jeon, G. Yoo, Y. Park, J. Lee, Y. Jang, J. Lee, S. Park, H. Yu, B. Shin, S. Lee, J. Park; *Adv. Mater.*, 2016, **28**, 864–870.
16 Y. Hong, D. Zhao, D. Liu, B. Ma, G. Yao, Q. Li, A. Han, M. Qiu, *Nano Lett.*, 2018, **18**, 5036.
17 Y. He, S. Liu, L. Kong, Z. Liu; *Spectrochimi. Acta A*, 2005, **61**, 2861.
18 A. Khawam and D. R. Flanagan; *J. Phys. Chem. B*, 2006, **110**, 17315.
19 X. Miao, S. Tongay, M. Petterson, K. Berke, A. Rinzler, B. Appleton, A. Hebard*; Nano Lett.* 2012, **12**, 2745.
20 Petr Vanýsek, Electrochemical Series, *CRC Handbook of chemistry and physics*, 2000.
21 K. Kurihara, J. Kizling, P. Stenius, J. Fendler; *J. Am. Chem. Soc.* 1983, **105**, 2574.
22 R. Phillipson, C. de la Rosa, J. Teyssandier, P. Walke, D. Waghray, Y. Fujita, J. Adisoejoso, K. Maili, I. Asselberghs, C. Huyghebaert, H. Uji-i, S. De Gendt, S. De Feyter., *Nanoscale*, 2016, **8**, 20017.
23 A. Johansson, P. Myllypekio, P. Koskinen, J. Aumanen, J. Koivistoinen, H. Tsai, C. Chen, L. Chang, V. Hiltunen, J.

Manninen, W. Woon, M. Pettersson, *Nano Lett.*, 2017, **17**, 6469.
24 H. Park, W. Jung, D. Kang, J. Jeon, G. Yoo, Y. Park, J. Lee, S. Park, H. Yu, B. Shin, S. Lee, J. Park; *Adv. Mater.*, 2016, **28**, 864-870.
25 E. Lee, K. Balasubramanian, R. Weitz, M. Burghard, K. Kern; *Nat. Nanotechnol.,* 2008, **3**, 486-490.
26 L. Wang, I. Meric, P. Huang, Q. Gao, H. Tran, T. Taniguchi, K. Watanabe, L. Campos, D. Muller, J. Guo, P. Kim, J. Hone, K. Shepard, C. Dean; *Science*, 2013, **342**, 614-617.
27 M. Khan, M. Iqbal, M. Iqbal, J. Eom; *Sci. Technol. Adv. Mat.,* 2014, **15**, 055004.
28 H. Pinto, A. Markevich; *Beilstein J. Nanotechnol.*, 2014, **05**, 1842-1848.
29. H. Zheng, S. Mukherjee, K. Gangopadhyay, S. Gangopadyay; *J. Mater. Sci: Mater. Electron.,* 2015, **26**, 4746-4753.